AFRL-ML-WP-TP-2007-456

MICROSTRUCTURE-SENSITIVE NOTCH ROOT ANALYSIS FOR Ni-BASE SUPERALLOYS (PREPRINT)

Yustianto Tjiptowidjojo, Mahesh Shenoy, Craig Przybyla, and David McDowell

MAY 2007

Approved for public release; distribution unlimited.

STINFO COPY

This work was funded in whole or in part by Department of the Air Force contract F33615-03-C-5229. The U.S. Government has for itself and others acting on its behalf an unlimited, paid-up, nonexclusive, irrevocable worldwide license to use, modify, reproduce, release, perform, display, or disclose the work by or on behalf of the U.S. Government.

MATERIALS AND MANUFACTURING DIRECTORATE
AIR FORCE RESEARCH LABORATORY
AIR FORCE MATERIEL COMMAND
WRIGHT-PATTERSON AIR FORCE BASE, OH 45433-7750

REPORT DOCUMENTATION PAGE

Form Approved
OMB No. 0704-0188

1. REPORT DATE *(DD-MM-YY)*	2. REPORT TYPE	3. DATES COVERED *(From - To)*
May 2007	Journal Article Preprint	

4. TITLE AND SUBTITLE
MICROSTRUCTURE-SENSITIVE NOTCH ROOT ANALYSIS FOR NI-BASE SUPERALLOYS (PREPRINT)

5a. CONTRACT NUMBER
F33615-03-C-5229

5b. GRANT NUMBER

5c. PROGRAM ELEMENT NUMBER
63211F

6. AUTHOR(S)
Yustianto Tjiptowidjojo, Mahesh Shenoy, Craig Przybyla, and David McDowell

5d. PROJECT NUMBER
3946

5e. TASK NUMBER
00

5f. WORK UNIT NUMBER
02

7. PERFORMING ORGANIZATION NAME(S) AND ADDRESS(ES)
Georgia Institute of Technology
School of Materials Science and Engineering
Atlanta, GA 30332-0405

8. PERFORMING ORGANIZATION REPORT NUMBER

9. SPONSORING/MONITORING AGENCY NAME(S) AND ADDRESS(ES)
Materials and Manufacturing Directorate
Air Force Research Laboratory
Air Force Materiel Command
Wright-Patterson AFB, OH 45433-7750

10. SPONSORING/MONITORING AGENCY ACRONYM(S)
AFRL-ML-WP

11. SPONSORING/MONITORING AGENCY REPORT NUMBER(S)
AFRL-ML-WP-TP-2007-456

12. DISTRIBUTION/AVAILABILITY STATEMENT
Approved for public release; distribution unlimited.

13. SUPPLEMENTARY NOTES
Journal article submitted to the International Journal of Engineering Science. This work was funded in whole or in part by Department of the Air Force contract F33615-03-C-5229. The U.S. Government has for itself and others acting on its behalf an unlimited, paid-up, nonexclusive, irrevocable worldwide license to use, modify, reproduce, release, perform, display, or disclose the work by or on behalf of the U.S. Government.

PAO Case Number: AFRL/WS 07-0634, 20 Mar 2007. This is the best copy available.

14. ABSTRACT
Macroscopic viscoplastic constitutive models for y-y Ni-base superalloys typically do not contain an explicit dependence on the underlying microstructure. Microstructure dependent models are of interest since the sizes, volume fractions, and morphologies of primary, secondary, and tertiary precipitates can substantially affect the stress-strain response. The principle microstructural features that can significantly affect the stress-strain response of y-y Ni-base superalloys are the grain size and precipitate volume fraction and size distributions. An Artificial Neural Network (ANN) is used to correlate the material parameters in an internal state variable cyclic viscoplasticity model with these microstructure plasticity calculations performed on other microstructures within the range characterized experimentally. The trained model is applied to an example of component notch root analyses to explore the potential impact of microstructure-sensitive constitutive models in fatigue design of structures.

15. SUBJECT TERMS
Nickel base superalloys, fatigue, microstructure, viscoplasticity models

16. SECURITY CLASSIFICATION OF:			17. LIMITATION OF ABSTRACT:	18. NUMBER OF PAGES	19a. NAME OF RESPONSIBLE PERSON (Monitor)
a. REPORT	b. ABSTRACT	c. THIS PAGE			Dallis Hardwick
Unclassified	Unclassified	Unclassified	SAR	30	19b. TELEPHONE NUMBER *(Include Area Code)* N/A

Standard Form 298 (Rev. 8-98)
Prescribed by ANSI Std. Z39-18

Microstructure-Sensitive Notch Root Analysis for Ni-Base Superalloys

To be submitted for Publication in the International Journal of Fatigue

Yustianto Tjiptowidjojo[1], Mahesh Shenoy[1*], Craig Przybyla[2], David McDowell[1,2†]
[1]The George W. Woodruff School of Mechanical Engineering
[2]School of Materials Science and Engineering
Georgia Institute of Technology
Atlanta, GA 30332-0405 USA

Abstract

Macroscopic viscoplastic constitutive models for γ–γ' Ni-base superalloys typically do not contain an explicit dependence on the underlying microstructure. Microstructure dependent models are of interest since the sizes, volume fractions, and morphologies of primary, secondary, and tertiary precipitates can substantially affect the stress-strain response. The principle microstructural features that can significantly affect the stress-strain response of γ–γ' Ni-base superalloys are the grain size and precipitate volume fraction and size distributions. An Artificial Neural Network (ANN) is used to correlate the material parameters in an internal state variable cyclic viscoplasticity model with these microstructure features using a combination of limited experiments augmented by polycrystal plasticity calculations performed on other microstructures within the range characterized experimentally. The trained model is applied to an example of component notch root analyses to explore the potential impact of microstructure-sensitive constitutive models in fatigue design of structures.

KEYWORDS: Nickel base superalloys; fatigue; microstructure; viscoplasticity models

---

* Corresponding author: Tel 404.894.5128; Fax 404.894.0186, Email: david.mcdowell@me.gatech.edu

† Currently at Schlumberger Reservoir Completions, Rosharon, TX

1. Introduction

Conventional macroscopic (referred to as 'macro') models for cyclic viscoplastic deformation do not typically contain explicit dependence on the underlying microstructure. Microstructure-sensitive models are of interest in view of variations of microstructure within heat-treated components. Moreover, components with functionally graded microstructures may exploit microstructure-property relations to achieve enhanced fatigue resistance. A microstructure-sensitive macroscopic internal state variable model (McDowell 2005a, 2005b) is useful since it is capable of giving microstructure-sensitive estimates of notch root cyclic stress-strain behavior of components.

The hierarchical methodology shown in **Figure 1** represents how this microstructural dependence has been embedded in the 'macro' model. In this work, constitutive models are formulated at two length scales: a lower scale internal state variable (ISV) dependent microscale model, which is formulated at the length scale of grains using the crystal plasticity framework (cf. Wang et al. 2007; Shenoy et al. 2007), and a macroscale ISV model. Virtual microstructure simulations from the microscale model are used to inform the microstructure dependent parameters in the macroscale model. There are three primary steps in the algorithm to embed microstructure dependence into the 'macro' model (Shenoy 2006; Shenoy *et al.* 2007):

- **Step 1** - A stress-strain database was generated for different strain histories using the polycrystal plasticity (referred to as 'micro') model for a range of microstructures that are intermediate to 7-8 selected actual microstructures used for 'micro' model calibration.
- **Step 2** – The Walker-type macroscopic ('macro') model parameters were determined for the stress-strain data for each microstructure in the database, including virtual microstructures intermediate to those experimentally characterized, using an optimization scheme.

- **Step 3** - An Artificial Neural Network (ANN) was trained to relate the parameters in the 'macro' model to the corresponding microstructural parameters. The microstructural features were varied randomly within the range shown in **Table 1**. A total of 150 microstructures were generated to train the ANN; more simulations could be run if desired.

The primary microstructural features that can significantly affect the cyclic stress-strain response of Ni-base superalloys are the grain size and the sizes and volume fractions of the Ni_3Al γ' precipitates, with ranges in the present Ni-base superalloy listed in Table 1. Both subsolvus and supersolvus heat treatments are considered. The response of this particular alloys is similar to IN 100 (Milligan et al. 2004), which was used in our prior study (Shenoy 2006; Shenoy et al. 2007).

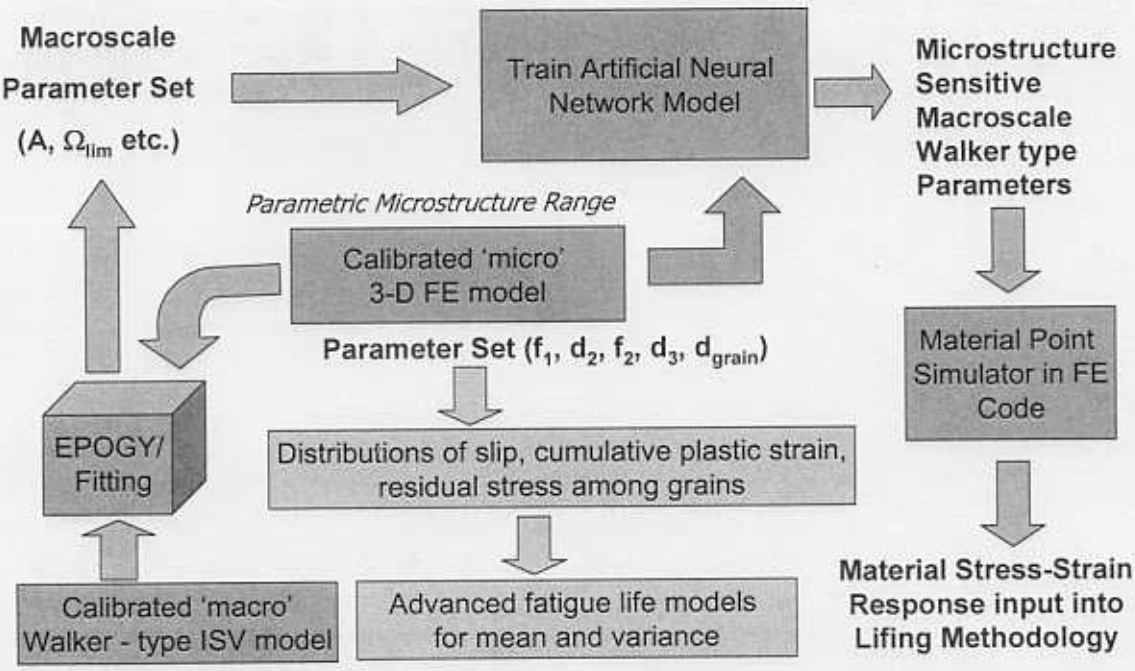

Figure 1. Framework for linking the 'micro' model to the 'macro' model.

Table 1. Ranges of microstructural features used to generate the database for 150 microstructures.

Microstructural Attribute	Min	Max
Volume Fraction of Primary γ' Precipitate, f_{p1}	0/0.07*	0.25
Volume Fraction of Secondary γ' Precipitate, f_{p2}	0.29	0.46
Secondary γ' Precipitate size, d_2 (nm)	110	340
Volume Fraction of Tertiary γ' Precipitate, f_{p3}	0.024	0.14
Tertiary γ' Precipitate size, d_3 (nm)	7.0	21.0
Grain Size, d_{grain} (microns)	4.0	34.0

*0 pertains to the case of no γ' primary precipitates; otherwise, minimum is 0.07.

2. 'Micro' Polycrystal Plasticity Model

Local crystal plasticity theory is used at the grain scale, with slip accounted for on both octahedral and cube slip planes in this class of alloys. The kinematical foundation for single crystal elastoplasticity has been built on a continuum perspective, (Asaro 1983a; 1983b). The deformation of a crystal is composed of contributions from (i) an overall "elastic" distortion of the lattice, and (ii) plastic deformation associated with dislocation glide that does not disturb the lattice geometry. The deformation gradient, $\underset{\sim}{F}$, is multiplicatively decomposed, i.e., $\underset{\sim}{F} = \underset{\sim}{F}^e \bullet \underset{\sim}{F}^p$. The linear hyperelastic relation (small elastic strains are assumed) is assumed at each temperature. The kinetics of shearing on each slip system is assigned as a function of resolved shear stress, with effects of initial yield and work hardening incorporated through micromechanical relations that reflect size-dependent precipitate shearing versus looping, and dislocation density evolution. The model equations are summarized in Table 2. The model is integrated over a large number of grains with random crystallite orientation distribution function that constitutes a Representative Volume Element for purposes of fitting complex cyclic deformation behavior of actual microstructures. Details may be found elsewhere and are beyond the scope of this paper (Shenoy 2006; Shenoy et al. 2007).

Table 2. Equations of the microstructure-sensitive ('micro') crystal plasticity model.

Flow Rule with Back Stress χ^{α}, Threshold Stress $\kappa_{\lambda}^{\alpha}$ and Drag Stress D^{α}

$$\dot{\gamma}^{\alpha}=\left[\dot{\gamma}_{o}\left\langle\frac{\left|\tau^{\alpha}-\chi^{\alpha}\right|-\kappa_{\lambda}^{\alpha}}{D^{\alpha}}\right\rangle^{n_1}+\dot{\gamma}_{1}\left\langle\frac{\left|\tau^{\alpha}-\chi^{\alpha}\right|}{D^{\alpha}}\right\rangle^{n_2}\right]\operatorname{sgn}\left(\tau^{\alpha}-\chi^{\alpha}\right)$$

where the threshold stress depends on dislocation density and particle shear resistance, i.e.,

$$\kappa_{\lambda}^{\alpha}=\kappa_{o,\lambda}^{\alpha}+\alpha_{t}\mu_{mix}b\sqrt{\rho_{\lambda}^{\alpha}}\quad\text{for }\lambda=\text{oct, cub}$$

$$\kappa_{o,oct}^{\alpha}=\left[\left(\tau_{o,\gamma}^{\alpha}\right)^{n_\kappa}+\psi_{oct}\left(f_{p1},d_2,f_{p2},d_3,f_{p3}\right)^{n_\kappa}\right]^{1/n_\kappa}+\frac{\left(f'_{p1}+f'_{p2}\right)}{f_{p\_ref}}\tau_{ns}^{\alpha}$$

$$\kappa_{o,cub}^{\alpha}=\left[\left(\tau_{o,\gamma}^{\alpha}\right)^{n_\kappa}+\psi_{cub}\left(f_{p1},d_2,f_{p2},d_3,f_{p3}\right)^{n_\kappa}\right]^{1/n_\kappa}$$

$$\tau_{ns}^{\alpha}=h_{pe}\tau_{pe}^{\alpha}+h_{cb}\left|\tau_{cb}^{\alpha}\right|+h_{se}\tau_{se}^{\alpha}$$

$$\psi_{oct}=\psi_{cub}=c_{p1}\sqrt{0.81wf'_{p1}\mu_{\gamma'}\frac{\Gamma_{APB}}{d_1}}+c_{p2}\sqrt{0.81wf'_{p2}\mu_{\gamma'}\frac{\Gamma_{APB}}{d_2}}+$$

$$c_{p3}\sqrt{\mu_{\gamma'}\frac{d_3}{d_{3ref}}f'_{p3}\frac{\Gamma_{APB}}{b}}+c_{gr}d_{gr}^{-0.5}$$

$$f'_{p1}=\frac{f_{p1}}{f_{p1}+f_m},f'_{p2}=\frac{f_{p2}}{f_{p2}+f_m},f'_{p3}=\frac{f_{p3}}{f_{p3}+f_m}$$

Internal State Variables at Slip System Level

a) Dislocation Density

$$\dot{\rho}_{\lambda}^{(\alpha)}=\sum_{\beta}h^{(\alpha\beta)}\left\{Z_o+k_1\sqrt{\rho_{\lambda}^{(\beta)}}-k_2\rho_{\lambda}^{(\beta)}\right\}\left|\dot{\gamma}^{(\beta)}\right|\qquad h^{\alpha\beta}=1$$

$$Z_o=\frac{k_\delta}{bd_{\delta eff}}\qquad d_{\delta eff}=\left(\frac{1}{d_{1\delta}}+\frac{1}{d_{2\delta}}\right)^{-1}$$

b) Back Stress

$$\dot{\chi}_{\lambda}^{(\alpha)}=C_{\chi}\left\{\eta\mu_s b\sqrt{\rho_{\lambda}^{(\alpha)}}\operatorname{sgn}\left(\tau^{(\alpha)}-\chi_{\lambda}^{(\alpha)}\right)-\chi_{\lambda}^{(\alpha)}\right\}\left|\dot{\gamma}^{(\alpha)}\right|\quad,\quad\eta=\frac{\eta_o Z_o}{Z_o+k_1\sqrt{\rho_{\lambda}^{(\alpha)}}}$$

3. 'Macro' Cyclic Viscoplasticity Model

3.1. *'Macro" Model Constitutive Equations*

In this section, the focus is on the general 3D formulation of the unified creep-plasticity internal state variable macroscopic model used to calculate the stress-strain response for different loading conditions. Under isothermal conditions, the rate of deformation tensor (true strain rate) $\underline{D}$ is decomposed into elastic and inelastic components, respectively identified by the superscripts e and n, i.e., $\underline{D} = \underline{D}^e + \underline{D}^n$. Under small strain conditions, the stress response is given by the material time derivative of the Cauchy (true) stress, i.e., $\overset{\circ}{\underline{\sigma}} = 2\mu \underline{D}^e + \lambda D^e_{kk} \underline{I}$, where μ and λ are the Lamé constants. Employing a two-term potential flow rule, the inelastic strain rate is written as

1. $$\underline{D}^n = f\left(\sqrt{\frac{3}{2}}\left\|\underline{\sigma} - \underline{\alpha}\right\|\right)\underline{n} = f\left(\sigma^v\right)\underline{n} = \dot{p}\,\underline{n} \tag{1}$$

with a two term flow potential, i.e.,

$$f\left(\sigma^v\right) = A_v\sqrt{\frac{3}{2}}\left\langle\frac{\sigma^v - \kappa - R}{D}\right\rangle^N + A_{v_2}\sqrt{\frac{3}{2}}\left\langle\frac{\sigma^v}{D}\right\rangle^{N_2} \tag{2}$$

and

$$\underline{n} = \frac{\underline{\sigma}' - \underline{\alpha}}{\left\|\underline{\sigma}' - \underline{\alpha}\right\|}, \quad \left\|\underline{\sigma}' - \underline{\alpha}\right\| = \left[\left(\underline{\sigma}' - \underline{\alpha}\right) : \left(\underline{\sigma}' - \underline{\alpha}\right)\right]^{1/2} \tag{3}$$

Here, $\underline{\sigma}'$ is the deviatoric part of the stress tensor, $\underline{\alpha}$ is the back stress tensor (deviatoric), and $\underline{\sigma}' - \underline{\alpha}$ is the overstress. The exponents N and N_2 indicate the rate sensitivity of each term in the flow rule. The use of two terms in the flow rule facilitates a multi-mechanism treatment of plastic flow at low and high stress levels. We set $N > N_2$ so that the first term in the flow rule is of quasi rate-independent character to capture the dominant cyclic behavior; the threshold stress

R plays a role in this dominantly athermal term. The second term largely represents effects of thermally activated flow at low stress levels and higher temperatures, and is used to model stress relaxation behavior. The two term potential may in itself be regarded as an approximation of the power law breakdown regime at higher strain rates (cf. Chaboche, 1989), thereby rendering the exponential terms nonessential (hence, we set $B_v = B_{v_2} = 0$). The constant D represents drag stress, and κ is the threshold stress. The material hardening derives from the dynamic equilibrium between competing hardening and dynamic recovery processes.

The term R corresponds to the isotropic hardening of the material (cf. Chaboche, 1985), i.e.

$$R = Q_h \left\{ 1 - \exp\left(-b_h \sqrt{\frac{2}{3}} p \right) \right\}, \quad p = \int \left\| D^n \right\| dt \tag{4}$$

which can be written in differential form as

$$\dot{R} = \left(E_1 - F_1 R \right) \sqrt{\frac{2}{3}} \dot{p}, \quad E_1 = Q_h b_h, F_1 = b_h \tag{5}$$

where Q_h is the saturation limit of the isotropic hardening, b_h controls the evolution rate, and p is the normed cumulative inelastic strain.

Assuming that the back stress tensor, $\underline{\alpha}$, is decomposed into two components (Moosbrugger and McDowell 1989, 1990), the kinematic hardening relation can be written as

$$\dot{\alpha} = \sum_{i=1}^{2} \left(\frac{2}{3} A_i \underline{n} - \sqrt{\frac{2}{3}} B_i \underline{\alpha}_i \right) \dot{p}, \quad B_i = \frac{A^i}{\alpha^i_{\lim}} \tag{6}$$

where A_i and B_i are respectively the direct hardening and dynamic recover rate coefficients, and $\alpha^i_{\lim}$ and is the saturation limit of the i^{th} component of back stress. It is noted that more complex forms involving nonlinear dynamic recovery can be introduced (cf. Ohno and Wang 1991a,

1991b; McDowell 1994, 1995; Abdel-Karim and Ohno 2000) if necessary to model cyclic ratcheting or progressive mean stress relaxation effects more accurately.

3.2. *Finite Element Implementation of the 'Macro" Model*

Either explicit or implicit integration algorithms can be used for time integration of the foregoing relations. For robustness with regard to time step, an implicit algorithm procedure is used. A residual for the flow rule in (1)-(3) may be rewritten as

$$g_i = \Delta p_i - \left(A_v \sqrt{\frac{3}{2}} \left\langle \frac{S_v}{D} \right\rangle^N \right)_i \Delta t - \left(A_{v_2} \sqrt{\frac{3}{2}} \left\langle \frac{S_{v_2}}{D} \right\rangle^{N_2} \right)_i \Delta t \tag{7}$$

The residual in Equation (7) should vanish at the end of the time step. To do this, the internal state variables ($\underset{\sim}{\alpha}, R$) have to be obtained at the end of the time step, which in turn depend on the inelastic strain increment; this necessitates an iterative procedure is needed here. A Newton-Raphson (N-R) scheme is employed for the root-finding procedure, with the algorithm described in the Appendix.

4. Microstructures

A matrix of potential γ -γ' microstructures that exhibit different average grain sizes as well as different sizes and volume fractions of the γ' precipitates. These microstructures are listed in **Table 3**. The definitions of the microstructural terms are listed in the first row in **Table 3**; f_{p1}, f_{p2}, and f_{p3}, are the volume fractions of the primary, secondary and tertiary γ' precipitates, respectively; d_1, d_2, and d_3 are the average diameters of the primary, secondary and tertiary γ' precipitates, respectively, and d_{grain} is the average grain size. The elastic behavior is assumed linear and isotropic, with Young's modulus, E_{mod} and elastic Poisson's ratio, ν.

For each microstructure, the 'macro' model parameters were obtained using the trained ANN (Shenoy 2006; Shenoy et al. 2007) and are tabulated in **Table 4**. The Neural Network Toolbox in MATLAB was used to perform the training using 150 simulation datasets. In this particular ANN, only two layers were used, a hidden layer and an output layer. The microstructure parameters are used as the input parameters and the 'macro' model parameters are used as the output variables.

Table 3. Features of model microstructures.

Microstructure	f_{p1}	d_1 (μm)	f_{p2}	d_2 (nm)	f_{p3}	d_3 (nm)	d_{grain} (μm)
M.1	0.1	1.0	0.45	150	0.1	15	31.8
M.2	0.1	1.0	0.45	250	0.1	15	31.8
M.3	0.1	1.0	0.3	200	0.2	15	31.8
M.4	0.1	1.0	0.45	250	0.1	15	4.0
M.5	0.1	1.0	0.45	250	0.1	15	16.0
M.6	0.1	1.0	0.45	250	0.1	15	30.0

Table 4. Macroscopic viscoplastic model parameters obtained from ANN (650°C).

Micro.	N	κ (MPa)	A_1 (MPa)	B_1	E_1 (MPa)	F_1	R_0 (MPa)
M.1	95	676	228000	1041	491	6.5	0
M.2	95	633	240000	1114	467	6.5	0
M.3	95	772	208000	960.6	575	6.5	0
M.4	95	755	278000	1064	499	6.5	0
M.5	95	721	257000	1114	493	6.5	0
M.6	95	646	242000	1114	468	6.5	0

Micro.	A_v (s^{-1})	D (MPa)	E_{mod} (MPa)	ν	A_2 (MPa)	B_2	$A_{v_2} \times 10^{-15}$ (s^{-1})	N_2
M.1	1.25×10^{-3}	250	158800	0.33	2256	5.6	132900	7
M.2	1.25×10^{-3}	250	158800	0.33	1640	4.1	210400	7

M.3	1.25×10^{-3}	250	156400	0.33	2584	6.5	287700	7
M.4	1.25×10^{-3}	250	158700	0.33	1915	4.8	320500	7
M.5	1.25×10^{-3}	250	158700	0.33	1739	4.3	273700	7
M.6	1.25×10^{-3}	250	158800	0.33	1643	4.4	216800	7

5. Geometry and Simulations

5.1 Notched Component Geometry, Mesh and Element Selection

The notched component (specimen) used for all the simulations is specified in **Figure 2**.

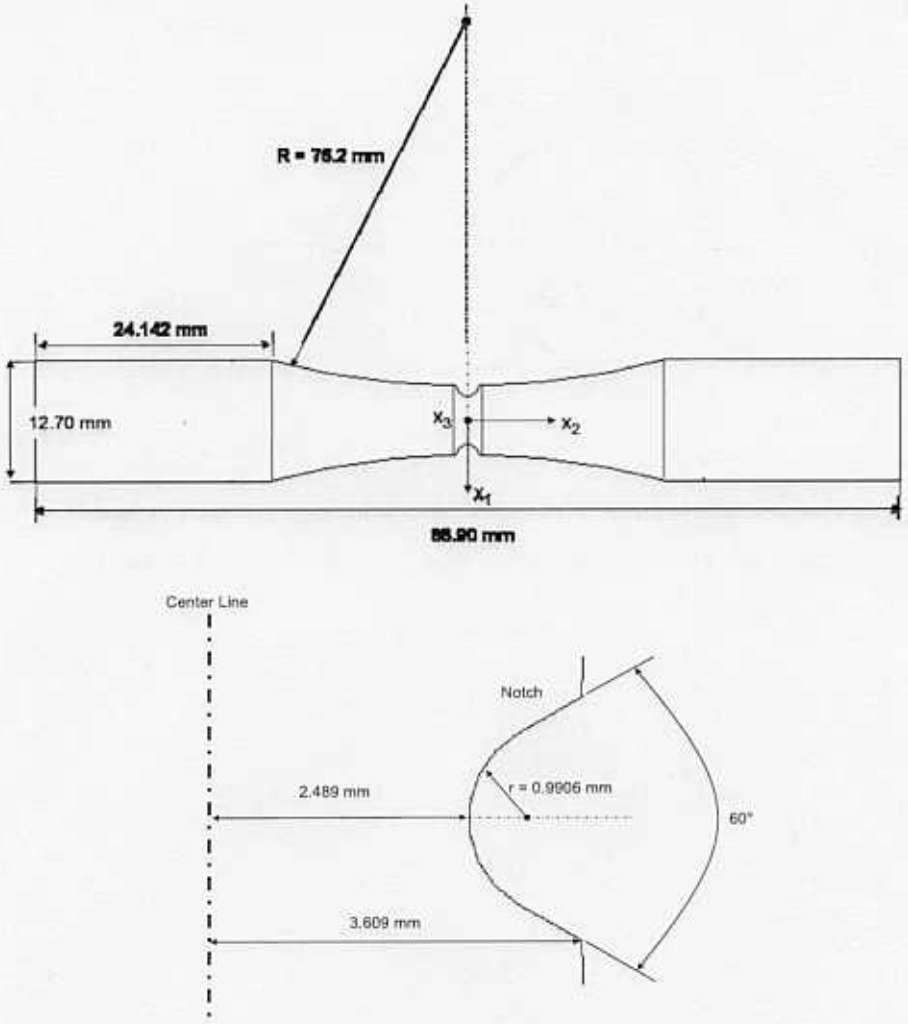

Figure 2. Specified geometry of notched specimens for 'macro' model FE simulations, showing details of notch root geometry in expanded view at bottom.

Axisymmetric elements were selected for the analyses as they provide the modeling of bodies of revolution under axially symmetric loading conditions. Both 4-node and 3-node continuum axisymmetric ABAQUS elements **CAX4** and **CAX3**, respectively, were utilized for all of the simulations.

Table 5. Comparison of different meshes tested to ensure convergence of the solution at the notch root.

Mesh	Elements	Axial Component of Plastic Strain (After 10 cycles)	Element Volume at Notch Root (μm^2)	Stress Concentration Factor (Elastic)
a	314	1.00%	67600	9.9
b	421	1.15%	38000	10.5
c	556	1.27%	16900	10.9
d	665	1.30%	12400	11.1
e	789	1.34%	9500	11.2
f	1045	1.37%	6000	11.5
g	1399	1.40%	4200	11.6
h	2927	1.45%	1500	11.9
i	5750	1.47%	380	12.1
j	3178	1.47%	200	12.1
Final	1055	1.46%	670	11.7

The component defined in **Figure 2** was modeled as axisymmetric. Several different meshes were compared to ensure that accurate results were obtained at the notch root. As seen in **Table 5**, the results converged when the area of the elements at the notch root were approximately 400 μm^2. It is noted that even though the area of the elements at the notch is less for each successive mesh from mesh a to j (see **Table 5**), the number of elements were reduced between meshes i

and j by coarsening elements further away from the notch to reduce computation time. In order to reduce computation time further, a mesh was selected with only 1055 elements using similar methods of fanning out the mesh across less critical regions; however, the area of the elements at the notch root were kept such that the maximum axial component of the plastic strain was within 1% of the result of the finest mesh tested. This mesh can be seen in **Figure 3.** The stress concentration factors as determined by the FEA simulations in the elastic regime are also shown in **Table 5**. An analytical elastic solution for the supplied geometry was not available.

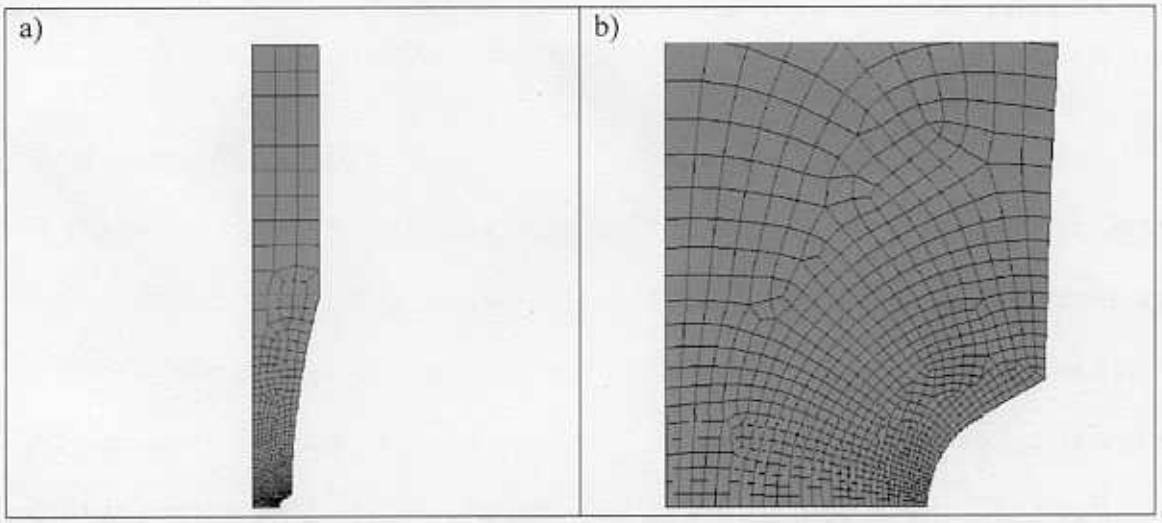

Figure 3. The final selected mesh used to model the notched component: a) complete mesh, and b) mesh in the vicinity of the notch root

5.2 Finite Element Simulations

FE Simulations were performed using the 'macro' UMAT for all the microstructures. For all simulations, isothermal conditions were assumed at 650°C. In addition, the FE simulations were all performed under nominal (in grips) stress control with R = 0.05. The load histories used in the FE simulations are listed in **Table 5**. Notch root stress-strain responses and associated accumulated plastic strain for all the microstructures are given in **Figures 4-11**. The accumulated

plastic strain at each point is defined as $\int_0^t \dot{\bar{\varepsilon}}^p dt$, with $\dot{\bar{\varepsilon}}^p = \sqrt{\frac{2}{3} D_{ij}^n D_{ij}^n}$. Calculations of nonlocal measures of notch root stress and strain were performed in all cases by averaging the values over a small but finite area of approximately 2500 μm^2 to provide an indication of the driving force for formation of small fatigue cracks of finite size, and to mitigate mesh dependencies of the solustions. These are the stress and strain values reported in **Figures 4-11.**

The sensitivity of responses to microstructure variation is interesting. For the shorter dwell times the creep resistance of microstructures (i.e., lowest accumulated plastic strain), listed in decreasing order, were M.4, M.3, M.5, M.1, M.6, and M.2, respectively. However for the longer hold times, the microstructures with the best creep resistance were M.1, M.4, M.6, M.2, M.5, and M.3, respectively. The largest difference in behavior between short and long hold times was observed for microstructure M.1, where the smaller size of the secondary precipitates and the larger grain size yielded better creep behavior for longer hold times than at shorter hold times. Microstructure M.1 had lower accumulated plastic strain for a short hold time.

Table 6. Strain histories used in FE simulations to compare response of various microstructures.

History	Temp (F)	Applied Nominal Max. Stress (MPa)	R	Ramp Up (s)	Ramp Down (s)	Peak Dwell (s)	Base Dwell (s)	CPM
1	1200.0	200.0	0.05	1.5	1.5	0.0	0.0	20.000
2	1200.0	200.0	0.05	15.0	15.0	90.0	0.0	0.500
3	1200.0	200.0	0.05	15.0	15.0	1200.0	0.0	0.049
4	1200.0	200.0	0.05	15.0	15.0	12000.0	0.0	0.005

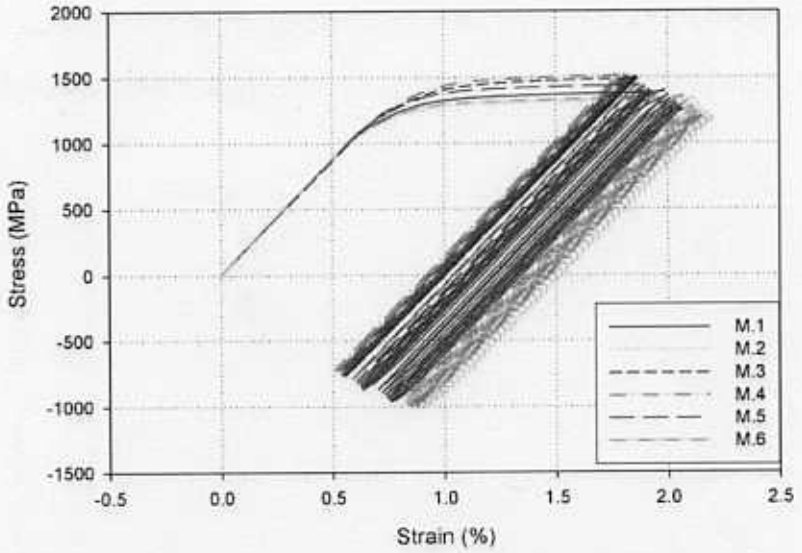

Figure 4. Comparison of notch root axial true stress (σ_{22}) versus axial true strain (ε_{22}) of all tested microstructures for microstructures M.1-M.6 for History 1.

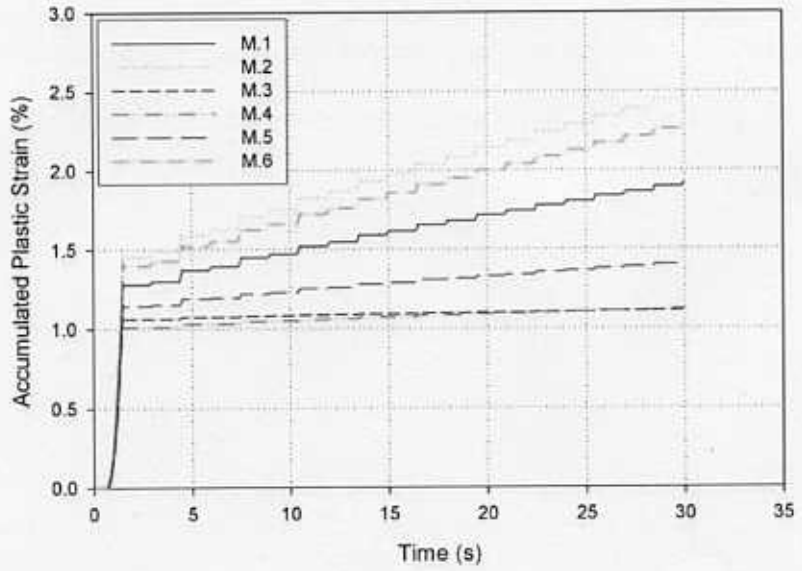

Figure 5. Comparison of notch root accumulated plastic strain ($\int_0 \dot{\bar{\varepsilon}}^P dt$) of all tested microstructures for microstructures M.1-M.6 for History 1.

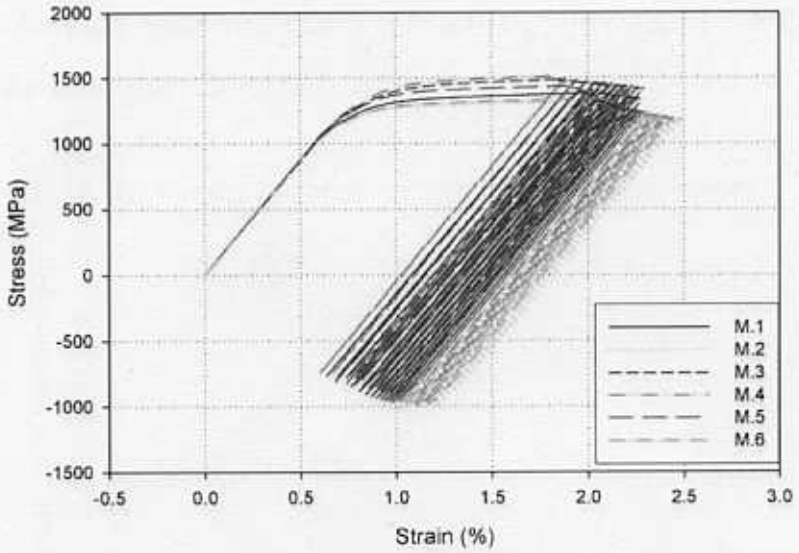

Figure 6. Comparison of notch root axial true stress (σ_{22}) versus axial true strain (ε_{22}) of all tested microstructures for microstructures M.1-M.6 for History 2.

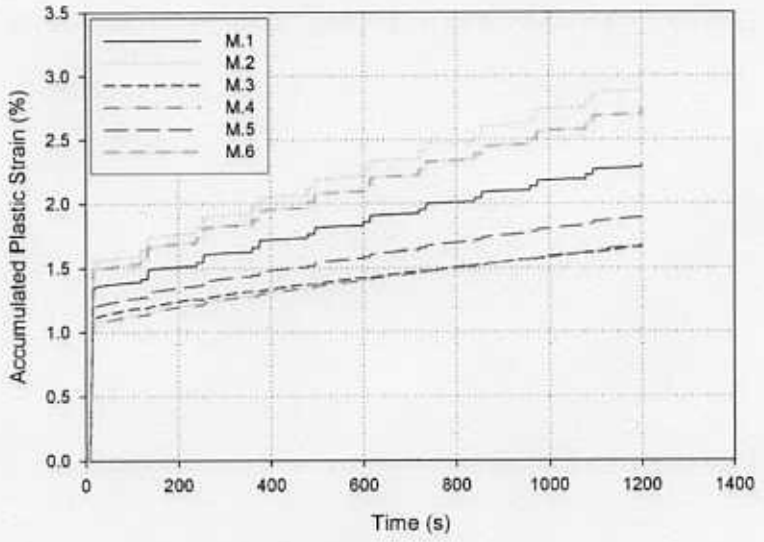

Figure 7. Comparison of notch root accumulated plastic strain ($\int_0^t \dot{\bar{\varepsilon}}^P dt$) of all tested microstructures for microstructures M.1-M.6 for History 2.

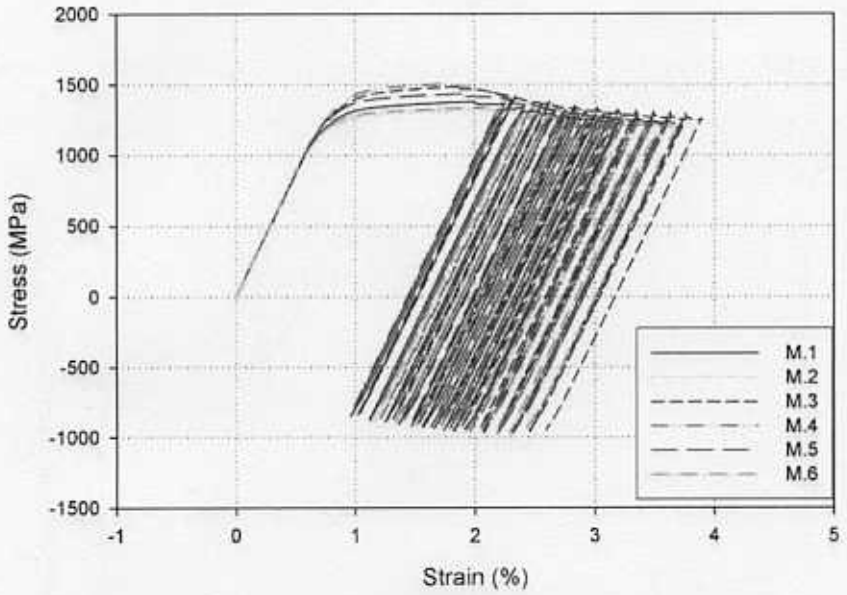

Figure 8. Comparison of notch root axial true stress (σ_{22}) versus axial true strain (ε_{22}) of all tested microstructures at notch root for microstructures M.1-M.6 for History 3.

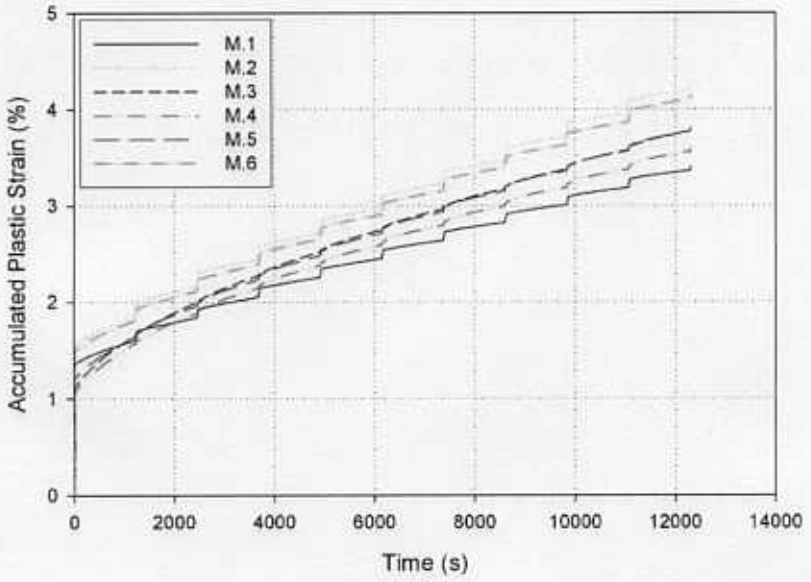

Figure 9. Comparison of notch root accumulated plastic strain ($\int_0^t \dot{\bar{\varepsilon}}^P dt$) of all tested microstructures for microstructures M.1-M.6 for History 3.

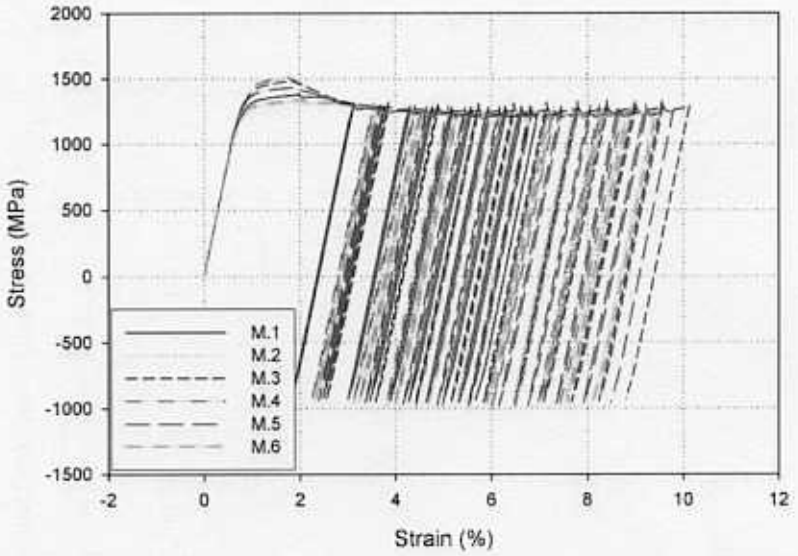

Figure 10. Comparison of notch root axial true stress (σ_{22}) versus axial true strain (ε_{22}) of all tested microstructures for microstructures M.1-M.6 for History 4.

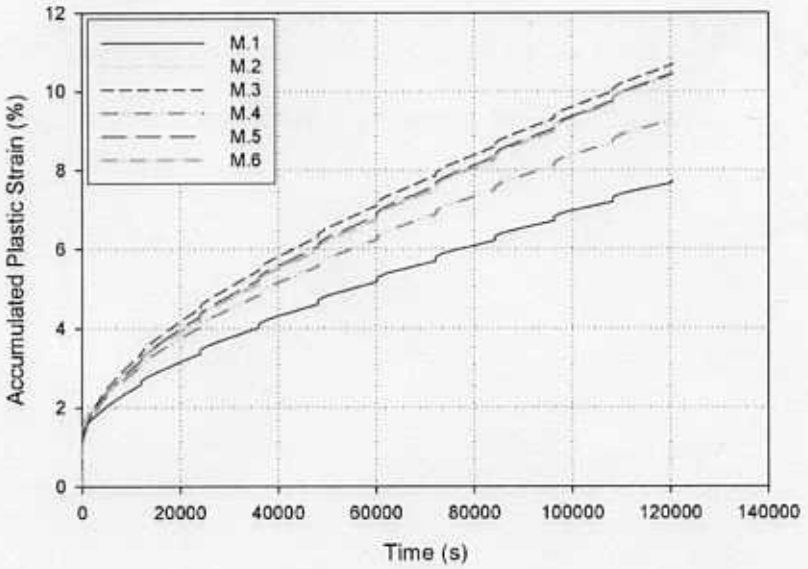

Figure 11. Comparison of notch root accumulated plastic strain ($\int_0^t \dot{\bar{\varepsilon}}^p dt$) of all tested microstructures for microstructures M.1-M.6 for Hstory 4.

Conclusions

Two important observations were made from this study:

- Using an artificial neural network to determine 'macro' material parameters to facilitate simulations of various microstructures is potentially useful in exploring effects of possible microstructure compositions on service behavior of components. The response of such 'engineered' microstructures can be projected before such materials are physically realized. Such studies can enable setting target volume fractions and precipitate sizes in the case of Ni-base superalloys.
- The sensitivity study of variation of notch root response with microstructures M.1-M.6 provided insight into the potential of the method outlined here for linking polycrystal plasticity calculations to macroscopic constitutive relations for use in notch root analyses. There is a pronounced effect of microstructure on mean stress relaxation, for example, that may impact fatigue life.

ACKNOWLEDGMENTS

This work was sponsored by the Pratt & Whitney (Project Manager Bob Grelotti) under subcontract from the US Air Force VAATE Program. The views and conclusions herein are those of the authors and should not be interpreted as necessarily representing the official policies or endorsements, either expressed or implied, of the US Air Force or PWA.

APPENDIX – Details of Numerical Implementation

Starting with the residual in Equation (7), we frame the N-R iteration as follows:

$$\Delta p_{i+1} = \Delta p_i - \frac{g_i}{\left[\partial g / \partial \Delta p\right]_i} \tag{A1}$$

The flow rule can be rewritten as

$$g = \Delta p - A_v \sqrt{\frac{3}{2}} \Delta t F\left(\underline{\sigma}', \underline{\alpha}, R\right) - A_{v_2} \sqrt{\frac{3}{2}} \Delta t F_2\left(\underline{\sigma}', \underline{\alpha}\right) \tag{A2}$$

where $F\left(\underline{\sigma}', \underline{\alpha}, R\right) = \left(\frac{\langle S_v \rangle}{D}\right)^N$, $F_2\left(\underline{\sigma}', \underline{\alpha}\right) = \left(\frac{\langle S_{v_2} \rangle}{D}\right)^N$. From chain rule differentiation,

$$\begin{aligned}
\frac{\partial g}{\partial \Delta p} &= 1 - A_v \sqrt{\frac{3}{2}} \Delta t \left(\frac{\partial F}{\partial \underline{\sigma}'} : \frac{\partial \underline{\sigma}'}{\partial \Delta p} + \frac{\partial F}{\partial \underline{\alpha}} : \frac{\partial \underline{\alpha}}{\partial \Delta p} + \frac{\partial F}{\partial R} \frac{\partial R}{\partial \Delta p} \right) \\
&\quad - A_{v_2} \sqrt{\frac{3}{2}} \Delta t \left(\frac{\partial F_2}{\partial \underline{\sigma}'} : \frac{\partial \underline{\sigma}'}{\partial \Delta p} + \frac{\partial F_2}{\partial \underline{\alpha}} : \frac{\partial \underline{\alpha}}{\partial \Delta p} \right) \\
&= 1 + F_v \left[\underline{n} : \left(2\mu \underline{n} + \frac{2}{3}\left(A_1 + A_2\right)\underline{n} - \sqrt{\frac{2}{3}}\left(B_1 \underline{\alpha}_1 + B_2 \underline{\alpha}_2\right) \right) + \frac{2}{3}\left(E_1 - F_1\right) R \right] \\
&\quad + F_{v_2} \left[\underline{n} : \left(2\mu \underline{n} + \frac{2}{3}\left(A_1 + A_2\right)\underline{n} - \sqrt{\frac{2}{3}}\left(B_1 \underline{\alpha}_1 + B_2 \underline{\alpha}_2\right) \right) \right]
\end{aligned} \tag{A3}$$

where

$$F_v = \frac{3}{2} A_v \Delta t \frac{N}{D} \left(\frac{\langle S_v \rangle}{D} \right)^{N-1}, \quad F_{v_2} = \frac{3}{2} A_{v_2} \Delta t \frac{N_2}{D} \left(\frac{\langle S_{v_2} \rangle}{D} \right)^{N_2 - 1} \tag{A4}$$

The inelastic strain increment and the internal state variables are updated using this scheme through successive iterates until $g_{i+1} \approx 0$ at the end of the time step.

The Newton-Raphson technique achieves a rapid convergence rate near the actual solution. However, it may diverge if the initial guess is sufficiently far from the actual solution. This

problem occurs when the values of $\underline{D}^n$ change significantly over a time step due to a large time step. Accordingly, a line search method proposed by Cuitiño and Ortiz (1992) is employed.

In addition, a time step subincrementation algorithm can also be supplemented to ensure convergence based on the work by Bennett (1999) and McGinty (2001). The implementation of the subincrementation method consists of "wrapping" a time step subincrementation routine around the Newton-Raphson and line search methods. If the Newton-Raphson with line search is not satisfactorily converging for a given time step, then the integration is performed in two smaller time steps, obtained by halving the original time step. The flow chart of this procedure is given in **Figure 12**.

The viscoplastic 'macro' constitutive model is coded as an ABAQUS 6.5-4 User MATerial subroutine (UMAT). ABAQUS provides the strain and Jacobian (the derivative of the stress with respect to elastic strain) matrices at the start of the time step, along with the overall strain and time increments for the step. The stresses, Jacobian matrix, and internal variables, which are history dependent, must be updated at the end of the time step in this UMAT. These values are returned to ABAQUS, which then continues equilibrium iteration. It is noted that the back stresses are not rotated at the end of the time step as would be required in a finite strain implementation, owing to relatively small cyclic strains of perceived applications. This could be added if necessary.

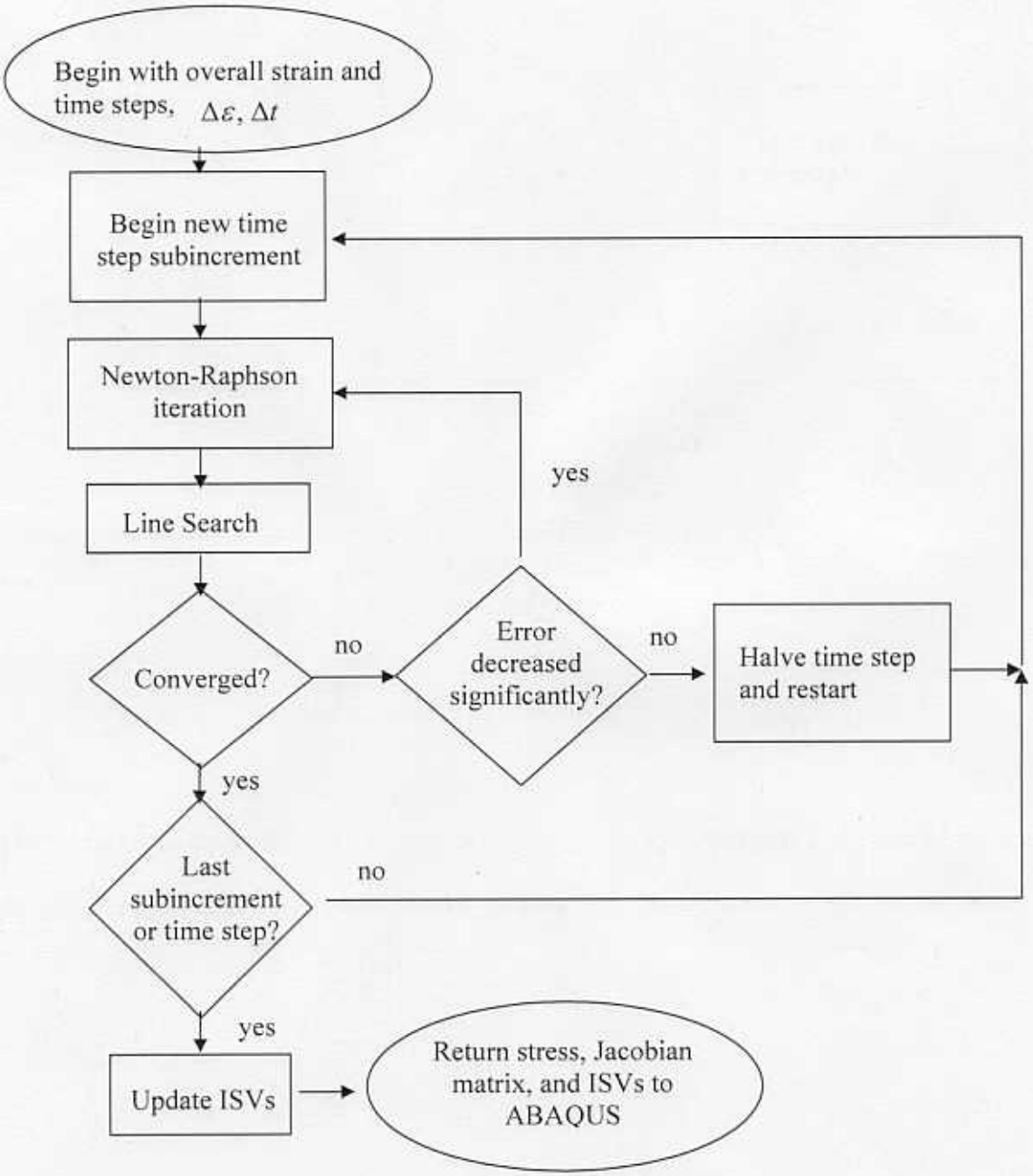

Figure 12. Flowchart of the constitutive law update in ABAQUS UMAT .

It is necessary to formulate the Jacobian matrix required by ABAQUS at the end of the time step for global equilibrium assessment. The Jacobian $\underset{\sim}{J}$ is given by

$$\underset{\sim}{J} = \frac{\partial \Delta \underset{\sim}{\sigma}}{\partial \Delta \underset{\sim}{\varepsilon}} = \frac{\partial}{\partial \Delta \underset{\sim}{\varepsilon}} \left[\underset{\sim}{C} : \left(\underset{\sim}{D} - \underset{\sim}{D}^{n} \right) \Delta t \right] = \underset{\sim}{C} - \left(\underset{\sim}{C} : \underset{\sim}{n} \right) \otimes \frac{\partial \Delta p}{\partial \Delta \underset{\sim}{\varepsilon}} \tag{A5}$$

The magnitude of the increment of plastic flow can be written as

$$\Delta p = A_{v} \sqrt{\frac{3}{2}} \Delta t F \left(\underset{\sim}{\sigma}', \underset{\sim}{\alpha}, R \right) + A_{v_2} \sqrt{\frac{3}{2}} \Delta t F_2 \left(\underset{\sim}{\sigma}', \underset{\sim}{\alpha} \right) \tag{A6}$$

Chain rule differentiation gives

$$\begin{aligned} \frac{\partial \Delta p}{\partial \Delta \underset{\sim}{\varepsilon}} = {} & A_{v} \sqrt{\frac{3}{2}} \Delta t \left(\frac{\partial F}{\partial \underset{\sim}{\sigma}'} : \frac{\partial \underset{\sim}{\sigma}'}{\partial \Delta \underset{\sim}{\varepsilon}} + \frac{\partial F}{\partial \underset{\sim}{\alpha}} : \frac{\partial \underset{\sim}{\alpha}}{\partial \Delta p} \otimes \frac{\partial \Delta p}{\partial \Delta \underset{\sim}{\varepsilon}} + \frac{\partial F}{\partial R} \frac{\partial R}{\partial \Delta p} \otimes \frac{\partial \Delta p}{\partial \Delta \underset{\sim}{\varepsilon}} \right) \\ & + A_{v_2} \sqrt{\frac{3}{2}} \Delta t \left(\frac{\partial F_2}{\partial \underset{\sim}{\sigma}'} : \frac{\partial \underset{\sim}{\sigma}'}{\partial \Delta \underset{\sim}{\varepsilon}} + \frac{\partial F_2}{\partial \underset{\sim}{\alpha}} : \frac{\partial \underset{\sim}{\alpha}}{\partial \Delta p} \otimes \frac{\partial \Delta p}{\partial \Delta \underset{\sim}{\varepsilon}} \right) \end{aligned} \tag{A7}$$

The contribution of the deviatoric stress-strain response to the Jacobian can be assessed by

$$\underset{\sim}{\sigma}' = \underset{\sim}{\sigma} - \frac{1}{3} \sigma_{kk} \underset{\sim}{I} \Rightarrow \quad \frac{\partial \Delta \underset{\sim}{\sigma}'}{\partial \Delta \underset{\sim}{\varepsilon}} = \frac{\partial \Delta \underset{\sim}{\sigma}}{\partial \Delta \underset{\sim}{\varepsilon}} - \frac{\partial}{\partial \Delta \underset{\sim}{\varepsilon}} \left(K \Delta \varepsilon_{kk} \underset{\sim}{I} \right) \tag{A8}$$

Since the last term is purely elastic response,

$$\frac{\partial \Delta \underset{\sim}{\sigma}'}{\partial \Delta \underset{\sim}{\varepsilon}} = \underset{\sim}{C} - \left(\underset{\sim}{C} : \underset{\sim}{n} \right) \otimes \frac{\partial \Delta p}{\partial \Delta \underset{\sim}{\varepsilon}} - K \left(\underset{\sim}{I} \otimes \underset{\sim}{I} \right) \tag{A9}$$

where $\underset{\sim}{C}$ is the elasticity tensor. Gathering results leads to the Jacobian

$$\underset{\sim}{J} = \underset{\sim}{C} - \left(\underset{\sim}{C} : \underset{\sim}{n} \right) \otimes \frac{\left(F_{v} + F_{v_2} \right) \underset{\sim}{n} : \left[\underset{\sim}{C} - K \left(\underset{\sim}{I} \otimes \underset{\sim}{I} \right) \right]}{1 + \mathbb{F}_1 + \mathbb{F}_2} \tag{A10}$$

where

$$\begin{aligned} \mathbb{F}_1 &= F_{v} \left[\underset{\sim}{n} : \left\{ \underset{\sim}{C} : \underset{\sim}{n} + \frac{2}{3} \left(A_1 + A_2 \right) \underset{\sim}{n} - \sqrt{\frac{2}{3}} \left(B_1 \underset{\sim}{\alpha}_1 + B_2 \underset{\sim}{\alpha}_2 \right) \right\} + \frac{2}{3} \left(E_1 - F_1 \right) R \right] \\ \mathbb{F}_2 &= F_{v_2} \left[\underset{\sim}{n} : \left\{ \underset{\sim}{C} : \underset{\sim}{n} + \frac{2}{3} \left(A_1 + A_2 \right) \underset{\sim}{n} - \sqrt{\frac{2}{3}} \left(B_1 \underset{\sim}{\alpha}_1 + B_2 \underset{\sim}{\alpha}_2 \right) \right\} \right] \end{aligned} \tag{A11}$$

REFERENCES

ABAQUS, Versions 6.5-4 and 6.6-1, 2005-2006. Abaqus, Inc., Providence, RI.

Abdel-Karim, M., Ohno, N. (2000). Kinematic Hardening Model Suitable for Ratchetting with Steady-State, *International Journal of Plasticity*, 16, 225-240.

Asaro, R.J., 1983a. Crystal plasticity. ASME J, Appl. Mech. **50**: 921-934.

Asaro, R.J., 1983b. Micromechanics of crystals and polycrystals. Adv. Appl. Mech. **23**: 1-115.

Bridgman, P.W. (1944). The Stress Distribution at the Neck of a Tension Specimen," Trans. ASM, 32 pp. 553-574.

Bridgman, P.W. (1964). *Studies in Large Plastic Flow and Fracture.* Harvard University Press, Cambridge, MA.

Chaboche, J.L. (1989). Constitutive equations for cyclic plasticity and cyclic viscoplasticity, *Int. J. Plast.*, 5, 247-302.

Jordan, E.H., Walker, K.P. (1992). A Viscoplastic Model for Single Crystals," *Journal of Engineering Materials and Technology*, 14, 19-26.

McDowell, D.L. (1992). A Nonlinear Kinematic Hardening Theory for Cyclic Thermoplasticity and Thermoviscoplasticity. *International Journal of Plasticity*. 8, 695-728.

McDowell, D.L. (1994). Description of Nonproportional Cyclic Ratchetting Behavior. *Eur. J. Mech., A/Solids*, 13, 593-604.

McDowell, D.L. (1995). Stress State Dependence of Cyclic Ratchetting Behavior of Two Rail Steels. *International Journal of Plasticity*, 11, 397-421.

McDowell, D.L. (2005a) Internal State Variable Theory. Handbook of Materials Modeling, Part A: Methods, eds. Sidney Yip and M.F. Horstemeyer, Springer, the Netherlands, 2005, pp. 1151-1170.

McDowell, D.L. (2005b) Microstructure-Sensitive Computational Fatigue Analysis. Handbook of Materials Modeling, Part A: Methods, eds. Sidney Yip and M.F. Horstemeyer, Springer, the Netherlands, 2005, pp. 1193-1214.

McGinty, R. D. (2001). *Multiscale Representation of Polycrystalline Inelasticity.* PhD Thesis, Georgia Institute of Technology.

Milligan, W.W., Orth, E.L., Schirra, J.J., Savage, M.F. (2004). Effects of microstructure on high temperature constitutive behavior of IN 100. Proc. Tenth International Symposium on Superalloys, 331-339.

Moosbrugger, J.C., McDowell, D.L. (1989). On a Class of Kinematic Hardening Rules for Nonproportional Cyclic Plasticity. *Journal of Engineering Materials and Technology*, 111, 87-98.

Moosbrugger, J. C., McDowell, D.L. (1990). A Rate Dependent Bounding Surface Model with a Generalized Image Point for Cyclic Nonproportional Viscoplasticity. *J. Mech. Phys. Solids*, 38, 627-656.

Moosbrugger, J. C., Morrison, D.J. (1997). Nonlinear Kinematic Hardening Rule Parameters – Direct Determination from completely Reversed Proportional Cycling. *International Journal of Plasticity*, 13, 633-668.

Ohno, N., Wang, J.D. (1991a). Transformation of a Nonlinear Kinematic Hardening Rule to a Multisurface form under Isothermal and Nonisothermal conditions. *International Journal of Plasticity*, 7, 879-891.

Ohno, N., Wang, J.D. (1991b). Two Equivalent forms of Nonlinear Kinematic Hardening: Application to Nonisothermal Plasticity. *International Journal of Plasticity*, 7, 637-650.

Pilkey, Walker. (1997). *Peterson's Stress Concentration Factors*. John Wiley & Sons, New York. Chart 2.19.

Shenoy, M. (2006). *Constitutive Modeling and Life Prediction in Ni-Base Superalloys*, PhD Thesis, Georgia Institute of Technology

Shenoy, M., Tjiptowidjojo, Y., McDowell, D.L. (2007) Microstructure-sensitive model for polycrystalline IN 100. To be submitted to the International Journal of Plasticity.

Stouffer D.C., Bodner, S.R. (1979). A constitutive model for the deformation induced anisotropic plastic flow of metal. *International Journal of Engineering and Science*, 17, 12-13.

Wang, A.-J., Kumar, R.S., Shenoy, M.M., and McDowell, D.L., 2007. Microstructure-based multiscale constitutive modeling of γ - γ' Nickel-base superalloys. International Journal of Multiscale Computational Engineering, in press.